Title

Helicobacter pylori cheV1 mutants recover semisolid agar migration due to loss of a previously uncharacterized Type IV filament membrane alignment complex homolog.

Journal

Journal of Bacteriology, 206(4)

Authors

Sagoo, Jashwin

Abedrabbo, Samar

Liu, Xiaolin

et al.

Publication Date

2024-04-18

DOI

10.1128/jb.00406-23

Peer reviewed

Journal of Bacteriology

Editor's Pick | Bacteriology | Full-Length Text

Helicobacter pylori cheV1 mutants recover semisolid agar migration due to loss of a previously uncharacterized Type IV filament membrane alignment complex homolog

Jashwin Sagoo,[1] Samar Abedrabbo,[1] Xiaolin Liu,[1] Karen M. Ottemann[1]

AUTHOR AFFILIATION See affiliation list on p. 11.

ABSTRACT The bacterial chemotaxis system is a well-understood signaling pathway that promotes bacterial success. Chemotaxis systems comprise chemoreceptors and the CheA kinase, linked by CheW or CheV scaffold proteins. Scaffold proteins provide connections between chemoreceptors and CheA and also between chemoreceptors to create macromolecular arrays. Chemotaxis is required for host colonization by many microbes, including the stomach pathogen *Helicobacter pylori*. This bacterium builds chemoreceptor–CheA contacts with two distinct scaffold proteins, CheW and CheV1. *H. pylori cheW* or *cheV1* deletion mutants both lose chemoreceptor array formation, but show differing semisolid agar chemotaxis assay behaviors: Δ*cheW* mutants exhibit total migration failure, whereas Δ*cheV1::cat* mutants display a 50% reduction. On investigating these varied responses, we found that both mutants initially struggle with migration. However, over time, Δ*cheV1::cat* mutants develop a stable, enhanced migration capability, termed "migration-able" (Mig^+). Whole-genome sequencing analysis of four distinct Δ*cheV1::cat* Mig^+ strains identified single-nucleotide polymorphisms (SNPs) in *hpg27_252 (hp0273*) that were predicted to truncate the encoded protein. Computational analysis of the *hpg27_252*-encoded protein revealed it encoded a hypothetical protein that was a remote homolog of the PilO Type IV filament membrane alignment complex protein. Although *H. pylori* lacks Type IV filaments, our analysis showed it retains an operon of genes for homologs of PilO, PilN, and PilM. Deleting *hpg27_252* in the Δ*cheV1::cat* or wild type strain resulted in enhanced migration in semisolid agar. Our study thus reveals that while *cheV1* mutants initially have significant migration defects, they can recover the migration ability through genetic suppressors, highlighting a complex regulatory mechanism in bacterial migration.

IMPORTANCE Chemotactic motility, present in over half of bacteria, depends on chemotaxis signaling systems comprising receptors, kinases, and scaffold proteins. In *Helicobacter pylori*, a stomach pathogen, chemotaxis is crucial for colonization, with CheV1 and CheW as key scaffold proteins. While both scaffolds are essential for building chemoreceptor complexes, their roles vary in other assays. Our research reexamines *cheV1* mutants' behavior in semisolid agar, a standard chemotaxis test. Initially, *cheV1* mutants exhibited defects similar to those of *cheW* mutants, but they evolved genetic suppressors that enhanced migration. These suppressors involve mutations in a previously uncharacterized gene, unknown in motility behavior. Our findings highlight the significant chemotaxis defects in *cheV1* mutants and identify new elements influencing bacterial motility.

KEYWORDS chemotaxis, flagellar motility, spontaneous mutations

Editor George O'Toole, Geisel School of Medicine at Dartmouth, USA

Address correspondence to Karen M. Ottemann, ottemann@ucsc.edu.

Jashwin Sagoo and Samar Abedrabbo contributed equally to this article. Author order was decided based on order of contribution to the project.

The authors declare no conflict of interest.

See the funding table on p. 11.

Received 4 December 2023
Accepted 21 February 2024
Published 6 March 2024

Bacterial motility is used to promote success in many environments, including during mammalian infections. Bacteria control motility, in part, via chemotaxis signal transduction systems that allow them to respond to harmful and helpful conditions and ultimately move toward beneficial situations (1–4). During chemotaxis, environmental factors such as amino acids, organic acids, and sugars are sensed by chemoreceptor proteins. These proteins in turn form complexes with the scaffold or coupling proteins CheW or CheV and the CheA kinase. Chemoreceptors act through the scaffold proteins to control CheA kinase activity, which phosphorylates CheY to create CheY-P. CheY-P then interacts with the flagellar motor and regulates its rotational direction. The chemoreceptor–scaffold–kinase complexes associate to form large macromolecular arrays, with 1,000 s of chemoreceptor–scaffold–kinase units. While the basic set of chemotaxis signaling proteins is conserved throughout bacteria, there are variations in terms of accessory proteins associated with each system (5). The study of these accessory proteins and non-canonical systems can provide insights into the working of chemotaxis signaling systems.

Chemotaxis signaling relies on chemotaxis scaffold proteins. The best-characterized scaffold is CheW, a small, two-domain protein that promotes two types of protein–protein interactions (6–8). The first is an interaction between chemoreceptors and CheA to allow control of the kinase. The second occurs between CheW proteins and promotes the formation of large chemoreceptor arrays. CheV scaffolds were discovered after CheW and are not as well-studied (6, 8). CheV proteins combine a CheW protein with an additional phosphorylatable response regulator domain. CheV proteins are capable of promoting the same protein–protein interactions as CheW (6, 8, 9). However, gaps still remain in our understanding of the CheV function as compared to CheW function.

H. pylori relies on chemotaxis signaling during its lifestyle. This microaerophilic Gram-negative microbe colonizes the human stomach, leading some people to develop gastritis, peptic ulcer disease, and stomach cancer (10, 11). This microbe requires motility and chemotaxis for full stomach colonization (12, 13). Specifically, mutants lacking core chemotaxis signaling proteins have significant colonization defects (14, 15).

The *H. pylori* chemotaxis system has a large number of scaffold proteins, including one CheW and three CheV proteins called CheV1, CheV2, and CheV3 (6, 12, 13). Of the CheV proteins, CheV1 plays a substantial role in chemotaxis, while CheV2 and CheV3 play only minor roles (15, 16). CheV1 operates similarly to CheW, with both creating protein–protein interactions to control CheA and build chemoreceptor arrays (9, 17). Mutational loss of either *cheW* or *cheV1* creates *H. pylori* that are unable to build chemoreceptor arrays having extreme flagellar biases consisting of forward swimming without reversals (9, 15). This phenotype is consistent with the loss of important scaffold proteins as without them, CheA cannot be activated or controlled, resulting in a concomitant loss of CheY-P. Consistent with these defects, *cheW*, *cheV1*, *cheA,* and *cheY* mutants have severe mouse colonization defects, being outcompeted 1,000-fold by wild-type *H. pylori* when co-inoculated (14, 15). Overall, this body of data suggests that both CheW and CheV1 play important roles in chemotaxis.

In contrast to their similarities, *cheV1* and *cheW* mutants display different phenotypes in a common chemotaxis assay, the semisolid (or soft) agar assay. In the semisolid agar assay, bacteria are inoculated at a single point, which then migrate to form a large colony if motile, chemotactic, and able to grow (18). In semisolid agar, *cheW* mutants have severe migration defects, equivalent to other fully non-chemotactic mutants such as those lacking *cheA* or *cheY* (15, 16). *cheV1* mutants, in contrast, have only an ~ 50% decrease in semisolid agar migration (15, 16). Of note, the loss of chemotaxis proteins in *H. pylori* does not create growth defects (14, 19), and both mutants are straight-swimming-biased (15). We were thus struck by this semisolid agar discrepancy. The previous chemotaxis semisolid agar assays were all carried out with relatively long incubation times, during which *H. pylori* genetic suppressors able to migrate have been documented to arise (20). We therefore wondered whether the semisolid agar phenotype of *cheV1* mutants, using a Δ*cheV1::cat* allele, might have been mischaracterized.

In this work, we reassessed the phenotypes of Δ*cheV1::cat* mutants and found that these mutants behave on semisolid agar in a manner that is consistent with full loss of chemotaxis initially, but with ready genetic suppression, resulting in variants able to migrate. Whole-genome sequencing identified that these variants had mutations in an uncharacterized open-reading frame *(hpg27_252*), a gene that was annotated as encoding a hypothetical protein with unknown function (21). The mutations in this gene caused either a truncation or a frameshift, predicted to result in the protein not being synthesized correctly. The role of *hpg27_252* was confirmed by targeted mutation, showing that elimination of this gene allowed recovery of Δ*cheV1::cat* mutant semisolid agar migration. Computational analysis revealed *hpg27_252*-encoded protein to be a remote ortholog of PilO, part of the Type IV filament cytoplasmic alignment complex. Our work thus suggests that *cheV1* mutants have equivalent defects to those of *cheW* ones, but readily regain suppressor mutations that allow migration. One such mutational site, in *hpg27_252*, encodes a previously unknown Type IV filament protein. This work is complemented by a sibling manuscript, Liu *et al*. (22).

RESULTS

cheV1 mutants have initial semisolid agar migration defects that lessen over time

CheV1 plays a pivotal role in forming *H. pylori* chemotaxis arrays (9). Given this role, it was surprising that *H. pylori cheV1* null mutants have only a partial semisolid agar migration defect (15, 16). The *H. pylori cheV1* null mutant semisolid agar phenotype was, therefore, studied over a course of time, using a previously generated *H. pylori* Δ*cheV1::cat* null mutant that replaces the open-reading frame with a chloramphenicol resistance cassette (*cat*), referred to as Δ*cheV1::cat* (15, 23). In this assay, wild-type (WT) bacteria form expanded colonies with large migration diameters, as opposed to non-motile or non-chemotactic bacteria (Che$^-$), which stay near the point of inoculation (18). After incubating for 4 days, the *H. pylori* Δ*cheV1::cat* mutant had a substantial migration defect, with colony diameters that were significantly below those of WT and not different from that of a Che$^-$ strain (Fig. 1A and B). The Δ*cheV1::cat* mutant phenotype changed over time, however, with an increased colony diameter that was still less than that of WT but significantly larger than that of Che$^-$ strains by day 7 (Fig. 1C and D). This outcome suggested that Δ*cheV1::cat* mutants had an initial soft agar defect that

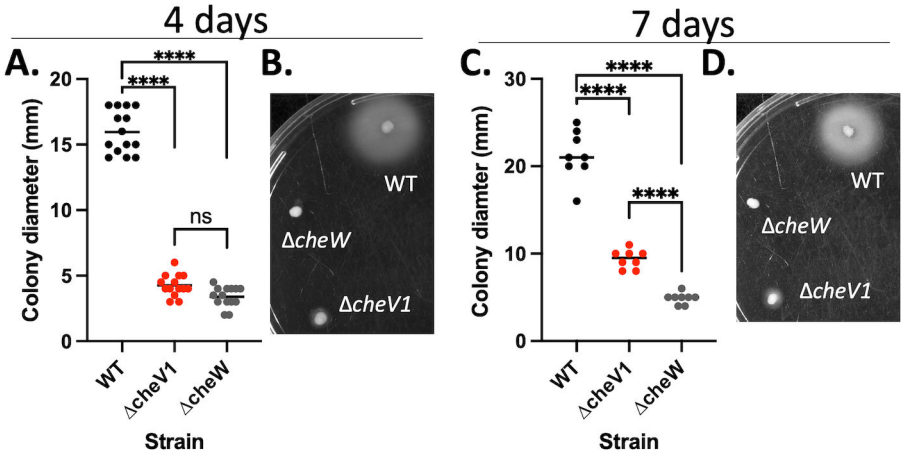

FIG 1 *cheV1* mutants have severe initial semisolid agar migration defects that lessen over time. Semisolid agar migration abilities were determined by wild-type G27 and its isogenic mutant strains. Bacteria were inoculated with a pipette tip into Brucella broth–FBS 0.35% agar plates and incubated at 37°C under microaerobic conditions. (A, C) Quantification of colony diameters in semisolid agar plates after 4 or 7 days, as indicated. *N* = 8–14 biological replicates/strain. Each point represents one colony measurement, and the bar indicates the mean. (B–D) Semisolid agar plate images of indicated *H. pylori* G27 strains after 4 or 7 days of incubation. Statistical analysis was performed using one-way ANOVA. **** indicates $P < 0.0001$.

may have been overcome. To assess whether this migration phenotype was genetically stable, we collected bacteria from the outer edges of the Δ*cheV1::cat* semisolid agar expansion, purified single colonies, and screened these individual strains on semisolid agar. The colony migration diameters of these strains were variable, but a significantly larger migration diameter than that of the Δ*cheV1::cat* parent strain or a Che$^-$ strain was observed (Fig. 2). These results suggested that the Δ*cheV1::cat* mutants may have acquired suppressor mutations that allowed for a significantly greater semisolid agar migration compared to the parent Δ*cheV1::cat* phenotype. These strains were termed Δ*cheV1* Mig$^+$ to indicate their phenotype of recovered migration on semisolid agar.

Δ*cheV1* Mig$^+$ strains display normal growth and do not change reversal frequency in liquid

Recovery of semisolid agar migration could arise through several mechanisms, as migration relies on a combination of growth, nutrient utilization, motility, and chemotaxis. We thus evaluated Δ*cheV1::cat* Mig$^+$ mutant growth and found it to be similar to that of WT and its Δ*cheV1::cat* parent (Fig. S1). We next examined bacterial swimming behavior as an indicator of flagellar rotational bias (20, 23). Δ*cheV1::cat* mutants displayed extremely few flagellar reversals and swam without direction changes, compared to WT (Fig. S2; Movies S1 and S2), as reported previously (15). Δ*cheV1::cat* Mig$^+$ variants similarly had few flagellar reversals in liquid media, nearly the same low-reversal phenotype as that of the Δ*cheV1::cat* mutant parent (Fig. S2; Movie S3). Overall, these results suggested

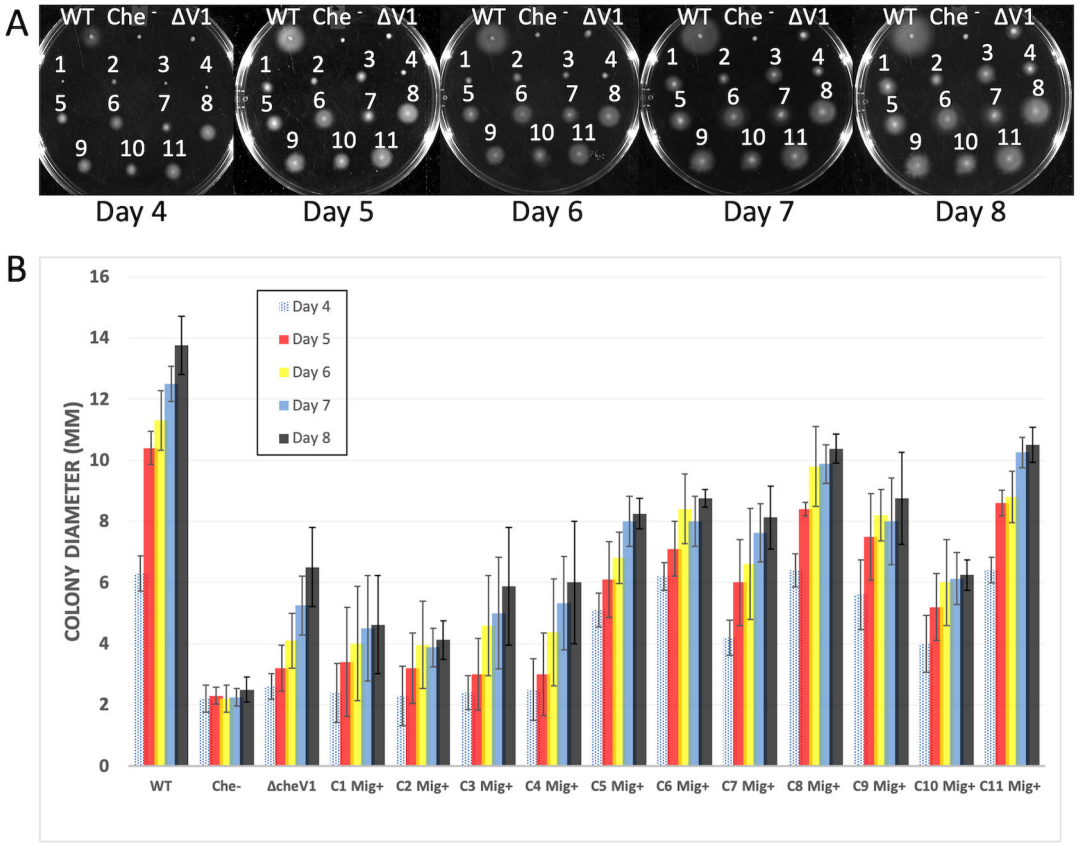

FIG 2 Δ*cheV1* Mig$^+$ suppressor colonies show improved soft agar migration. Semisolid agar migration abilities were determined as described in Fig. 1. Numbered colonies represent colony-purified isolates of Δ*cheV1* mutants collected from the outer edge of the bacterial growth halo on semisolid agar plates after 5–6 days. (A) Images of Brucella broth–FBS semisolid agar plates incubated for 4–8 days. Numbers indicate the Δ*cheV1* suppressor colonies. (B) Quantification of colony diameters in soft agar plates. Colonies C5, C6, C8, and C11 were genome-sequenced. Data are shown as a mean, and error bars represent standard deviation (n = 9–12 for all strains).

that the Δ*cheV1::cat* Mig$^+$ suppressors did not acquire their semisolid agar migration phenotype by affecting known behaviors such as growth rate or flagellar reversals.

Genomic sequencing of four Mig$^+$ suppressors reveals acquired SNPs in HPG27_252

To gain an insight into the basis of the Δ*cheV1::cat* Mig$^+$ phenotype, we determined the full genomic sequences of four Mig$^+$ suppressors (numbers 5, 6, 8, and 11 in Fig. 2) and the *H. pylori* G27 Δ*cheV1::cat* parent. These sequences were compared to those of the published *H. pylori* G27 reference genome (21). Multiple single-nucleotide polymorphisms (SNPs) were discovered across these suppressors when mapping the sequencing data to the reference genome (Table S1), but one locus stood out because it had distinct SNPs in each of the four Δ*cheV1::cat* Mig$^+$ strains that were not present in the Δ*cheV1* parent (Table S1). This locus, *hpg27_252* [*hp0273* in the reference *H. pylori* 26695 genome (24)] had SNPs in different positions, but all were predicted to truncate the encoded protein (Fig. 3). HPG27_252 is annotated as a hypothetical protein in the original *H. pylori* G27 genome annotation (21) but was reannotated by an automated process at the NCBI as a pseudogene. We thus carried out Sanger sequencing of PCR products of this region and confirmed that the gene is intact in the Δ*cheV1::cat* parent and indeed contained SNPs in the Mig$^+$ variants. Taken together, these data suggested that *hpg27_252* is a site of mutations in Δ*cheV1::cat* Mig$^+$ suppressors.

hpg27_252 encodes an inner membrane protein with remote homology to Type IV filament cytoplasmic membrane complex members

The *hpg27_252* encoded protein was analyzed using bioinformatic tools. During the genome and Sanger sequencing, we identified an error, of a missing adenine nucleotide, in the original G27 genome for this gene, which truncated the protein after ~2/3 of the gene. Data from both the Δ*cheV1::cat* mutant parent and the four suppressor colonies supported that this was an error in the reference genome. The corrected sequence resulted in a longer open-reading frame of 179 amino acids. The *hpg27_252* gene is conserved in all *H. pylori* genomes, with the predicted open-reading frames encoding the longer, 179-amino acid version (Fig. S3). This conservation combined with the sequencing supports that the longer gene is correct. The encoded full-length protein has a predicted 24-amino acid N-terminal region, a predicted transmembrane domain from amino acids 25–34, and a C-terminal periplasmic domain from amino acids 35–179 (Fig. 4). BLAST and BLASTp with HPG27_252 yielded no significant hits to proteins with known functions, whereas Pfam identified only an uncharacterized DUF, DUF5401. We therefore utilized HHpred searches to identify remote homologs based on statistical models. This approached identified PilO and PilN proteins (Table 1).

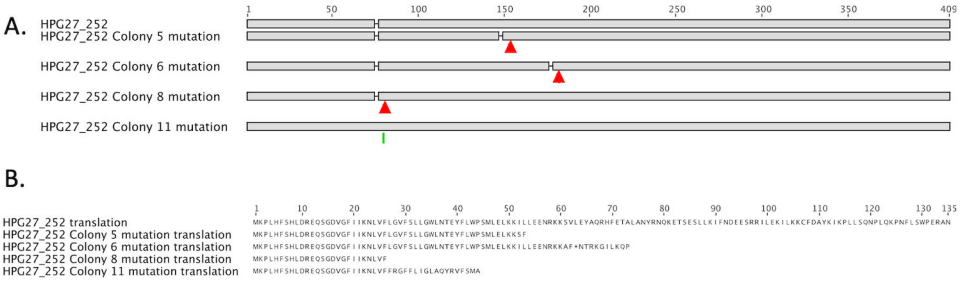

FIG 3 *hpg27_252* is mutated in *cheV1* Mig$^+$ suppressor mutants. (A) Locations of mutations in the *hpg27_252* gene for colony 5 (deletion), 6 (deletion), 8 (deletion), and 11 (insertion). The top line represents *hpg27_252* from the G27 reference sequence (21), with a dash inserted for the alignment with colony 11. (B) Representations of the translation of HPG27_252 WT, which encodes a 135-amino acid protein in the G27 reference genome. The four mutations all cause frameshifts that truncate and alter the resulting product.

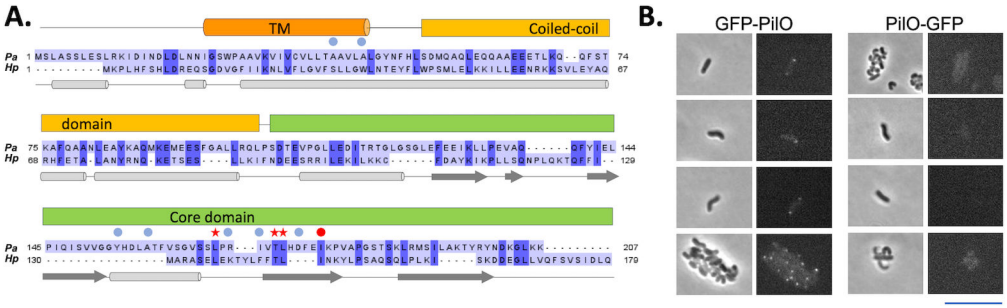

FIG 4 HPG27_252 alignment and topology show similarities to other PilO proteins. (A) Alignment of *H. pylori* HPG27_252 and *Pseudomonas aeruginosa* PilO. The numbers on the left and right of each sequence show the positions of the residues. Conserved amino acids are highlighted with dark blue. The *P. aeruginosa* PilO domain organization is shown above the amino acid sequences and the secondary structure below. Three conserved important sites of *P. aeruginosa* PilO present in *H. pylori* PilO are shown with red stars (25, 26). Other sites important for *P. aeruginosa* PilO function are marked with circles, red for conserved with *H. pylori* PilO or blue if not. (B) Localization of GFP-PilO and PilO-GFP in *H. pylori* G27. Representative pictures of GFP-PilO localization (left panel) and PilO-GFP localization (right panel). The left and right sides of each panel show a brightfield and a fluorescence microscopy image, respectively. Scale bar = 5 µm.

PilO, PilN, and related proteins like GspM are part of the cytoplasmic membrane alignment complex of Type IV filament (TFF) nanomachines, typified by Type IV pili (T4P) and Type II secretion systems (T2SS) (23, 24, 28). Both of these types of filaments form structures that extend from the cytoplasmic membrane to outside the cell, serving various functions, including adhesion, extension–retraction-based motility, and protein secretion. *H. pylori* is not known to have any T4P or T2SS (21, 24, 28, 29). However, in support of the idea that hpg27_252 encodes a bona fide PilO homolog, we analyzed the gene neighborhood and found that the genes that are predicted to be co-transcribed with *hpg27_252*, based on analysis in strain 26695 (30), also encode predicted components of the T4P cytoplasmic membrane alignment complex, PilN and PilM, with an overlapping gene arrangement that suggests the protein products may interact (Fig. S3). This result provides further evidence that *hpg27_252* encodes a homolog of TFF proteins.

To further explore the relationship between HPG27_252 and T4P PilO, we aligned the sequence of HPG27_252 and the well-studied *P. aeruginosa* PilO (25, 26). *H. pylori* HPG27_252 and *P. aeruginosa* PilO showed significant similarity (36.6%) (Fig. 4). L167, T172, and L173 sites in the most highly conserved region (LPRIVTL) of *P. aeruginosa* PilO (25, 26) are present in HPG27_252. The PilO I178 site affecting *P. aeruginosa* TFP function (2) is also present in HPG27_252. We also explored the predicted protein topology by fusing GFP to the predicted cytoplasmic N or predicted periplasmic C-terminus of HPG27_252. The N-terminal GFP fusion resulted in visible fluorescence (Fig. 4B), which

TABLE 1 HPG27_252 homology to PilO and PilN[a]

Query	Hit	Hit name	Prob	*E*-value	Aligned
HPG27_252/HP0273	3JC8_NI	PilN *Myxococcus xanthus* DK 1622	98.9	1.7E-06	47–177
	3JC9_Oi	PilO *Myxococcus xanthus* DK 1622	98.9	6.7E-06	20–177
HPG27_251/HP0272	3JC8_NI	PilN *Myxococcus xanthus* DK 1622	99.73	3.8e-15	15–139
	4BHQ_B	PilN *Thermus thermophilus*	99.43	3.3e-11	44–146
	3JC9_Oi	PilO; *Myxococcus xanthus* DK 1622	99.13	1.2e-8	25–52
HPG27_250/HP0271	3WT0_C	FtsA; Cell division protein *Staphylococcus aureus*	92.53	11	1–305
	3HRG_A	BT_3980 uncharacterized protein with actin-like ATPase fold; *Bacteroides thetaiotaomicron* BT_3980,	91.93	12	19–191
	2YCH_A	PilM *Thermus thermophilus*	90.57	17	1–305

[a]Remote homologs of HPG27_252, HPG27_251, and HPG27_250 were identified using HHpred from the MPI Bioinformatics Toolkit (27). Hit indicates the matched protein ID in the RCSB protein data bank (https://www.rcsb.org/structure/3JC8). Hit name indicates a short description of the matched protein. Probability and *E*-value indicate the estimated probability that the template hit is homologous to the query. Probability scores are calculated to include the secondary structure similarity, with scores greater than 95% indicating the homology is highly certain. *E*-value is an alternative measure of statistical significance that does not include the secondary structure and is therefore described as less sensitive than the probability score. Aligned indicates the region in the query that matched the hit.

was not present in the C-terminal GFP fusion (Fig. 4B). These results suggest that HPG27_252 in *H. pylori* may have a shared topology and mechanism with PilO homologs.

Elimination of *hpg27_252* results in enhanced migration in the Δ*cheV1* and WT strains

Given that Δ*cheV1::cat* Mig$^+$ suppressors have SNPs in *hpg27_252* that truncated the protein, we explored whether loss of the *hpg27_252* gene would be sufficient to allow Δ*cheV1::cat* mutants to improve semisolid agar migration. We thus replaced the majority of *hpg27_252* with a kanamycin resistance gene in the Δ*cheV1::cat* background and examined the migration behavior of the resultant strain in semisolid agar. The colony diameter of these strains was larger than that of the Δ*cheV1::cat* parent, supporting the role of this gene in the phenotype of the Δ*cheV1::cat* Mig$^+$ suppressors (Fig. 5A). In addition, we examined how the loss of *hpg27_252* would affect WT migration and found that this mutation also enhanced WT migration (Fig. 5B and C). The *hpg27_252* mutant phenotype was complemented by the introduction of a plasmid copy of *hpg27_252* (Fig. 5B and C), supporting the idea that loss of *hpg27_252*, and not polar effects, conferred enhanced semisolid agar migration.

DISCUSSION

We report here that *H. pylori cheV1* mutants indeed have substantial chemotaxis defects and are poorly able to migrate in the semisolid agar chemotaxis assay. These mutants readily accumulate genetic suppressors, however, giving the appearance of having reasonable migration abilities. Here, we identified that Δ*cheV1::cat* mutants gain improved migration ability due to mutational inactivation of an uncharacterized gene, *hpg27_252*. Mutants lacking this gene allow enhanced semisolid agar migration of Δ*cheV1::cat* mutants and the WT parent. HPG27_252 and its orthologs encoded in other *H. pylori* genomes are annotated as hypothetical proteins. Our analysis here suggests that this gene's product as well as the others in its operon represent remote homologs of the Type IV filament cytoplasmic membrane alignment complex.

The *cheV1* mutant semisolid agar migration phenotype prior to this work was unclear. Δ*cheV1* mutants had previously been reported to have ~40% ability to migrate in semisolid agar (15, 16). *H. pylori* semisolid agar assays are typically incubated for 4–8 days, a time during which second-site suppressor mutations have been reported to arise

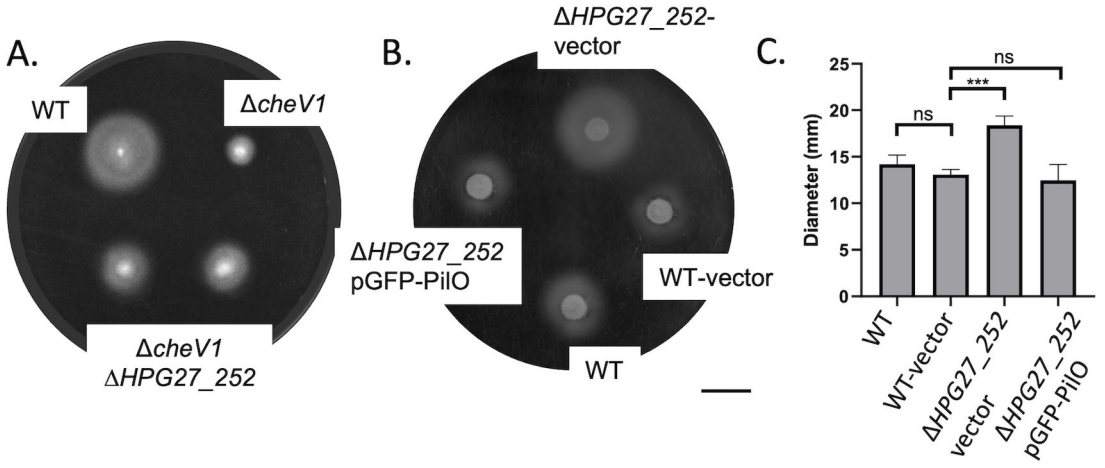

FIG 5 Loss of *hpg27_252* in the Δ*cheV1* mutant allows semisolid agar migration recovery. *hpg27_252* was deleted and replaced by a kanamycin resistance cassette in the *H. pylori* Δ*cheV1* background. Semisolid agar migration as assessed after days, using Brucella broth–FBS semisolid agar plates. (A) Δ*hpg27_252* was deleted in the Δ*cheV1* background. Two biological replicates of Δ*hpg27_252* Δ*cheV1* are shown. (B) Δ*hpg27_252* was deleted in the WT background and then complemented with a plasmid-bearing *hpg27_252* or vector alone. In panels A and B, plates are representative of three to five independent biological replicates. Scale bar = 10 mm. (C) Quantification of complementation shown in panel B. The asterisks indicate significant differences with WT or between two strains, as indicated with lines according to the one-way ANOVA (***, $P < 0.001$; ns, no significant difference).

(20). During our experiments, we noticed that Δ*cheV1::cat* mutants had a strong early defect that appeared to lessen over time. This observation provided the impetus for this work, to carefully characterize the Δ*cheV1* mutant phenotype. Indeed, we found that *cheV1* mutants are equivalent to other non-chemotactic mutants in the first 3–5 days of semisolid agar migration. These results thus suggest that *cheV1* mutants do have strong semisolid agar migration defects, consistent with CheV1's important role in forming chemoreceptor arrays (9).

After several days of semisolid agar incubation, Δ*cheV1::cat* mutants accumulated SNPs in the *hpg27_252* gene. The SNPs consisted of distinct insertions or deletions that resulted in a truncated open-reading frame lacking most of its predicted periplasmic domain. Complete deletion of *hpg27_252* enhanced *cheV1* mutant semisolid agar migration, supporting the hypothesis that removal of *hpg27_252* allows enhanced migration. Indeed, loss of this gene also enhanced WT migration. The targeted *hpg27_252* mutant, however, did not allow full WT migration, suggesting there may be other mutations in the Δ*cheV1::cat* Mig$^+$ background or that the first ~23 amino acids of HPG27_252 play a role. The fact that loss-of-function mutations allow better migration fits well with the apparent high frequency of this occurrence.

It is not yet known why the loss of HPG27_252 confers enhanced semisolid agar migration. *hpg27_252* encodes a remote homolog of TFF proteins PilO or GspM that compose the cytoplasmic membrane alignment complex found in T4P and T2SS (31, 32). Both PilO and GspM are cytoplasmic membrane proteins with substantial periplasmic domains that adopt a ferredoxin-like fold. PilO and GspM form homodimers and heterodimers with PilN/GspL and create a cage-like ring structure. The exact function, however, remains unknown other than hypothesized ones to control TFF dynamics or align the cytoplasmic components with those at the outermembrane. The *hpg27_252* gene is part of an operon with two other genes predicted to encode portions of the cytoplasmic membrane alignment complex, *pilN* (HPG27_251) and *pilM* (HPG27_250), and these genes are found in all *H. pylori* genomes. *H. pylori* does not have any reported T4P or T2SS nor are any other genes for these processes near the locus identified here, suggesting that these TFF remote orthologs may be isolated and possibly used for processes other than the creation of TFF.

Recovery of semisolid agar migration is a powerful selection and has led to the identification of new proteins involved in motility and chemotaxis (33). For example, Terry *et al*. used semisolid agar migration recovery in *H. pylori cheW* mutants to identify that *H. pylori* had a previously unknown remote homolog of the CheZ chemotaxis phosphatase and expanded our understanding of the distribution of this protein (20, 34). In some cases, the migration-gaining strains are pseudo-revertants, meaning they occur outside the originally targeted gene. Semisolid agar pseudo-revertants include mutations that affect flagellar reversals as a way to override migration due to chemotaxis defects (35, 36). Studies on how HPG27_252 allows semisolid agar migration will be informative, as its loss does not revert the extreme counterclockwise bias of Δ*cheV1* mutants and also enhances WT migration. This work has identified a new player in *H. pylori* semisolid agar behavior; understanding its function will shed new light on this process.

MATERIALS AND METHODS

Bacterial strains and culture conditions

H. pylori G27 (21, 37), Δ*cheV1::cat* mutant (15) and other strains and plasmids used in this study are listed in Table S2. *H. pylori* strains were grown on solid media consisting of Columbia agar with 5% v/v defibrinated horse blood (Hemostat Labs) with antibiotics at final concentrations of 50 µg/mL cycloheximide, 10 µg/mL vancomycin, 5 µg/mL cefsulodin, 2.5 units/mL polymyxin B, 5 µg/mL trimethoprim, and 8 µg/mL amphotericin B (CHBA). For mutant selection, chloramphenicol was used at 13.33 ug/mL, and kanamycin was used at 15 ug/mL. The plates were incubated at 37°C in a microaerobic

incubator with 10% v/v CO_2, 5% v/v O_2, and 85% v/v N_2. Liquid cultures of *H. pylori* were grown in Brucella broth supplemented with 10% v/v heat-inactivated fetal bovine serum (FBS) supplemented with antibiotics mentioned previously (BB10). *E. coli* strains were grown on LB plates with 100 µg/mL ampicillin or 60 µg/mL kanamycin antibiotics under normoxic conditions at 37°C. For long-term storage, *H. pylori* was mixed with brain–heart infusion broth with 10% FBS, 1% (wt/vol) beta-cyclodextrin, 25% glycerol, and 5% DMSO and frozen at –80°C. To measure growth rates, strains were grown in BB10 without antibiotics overnight.

Semisolid agar assays and isolation of Mig$^+$ suppressors

Semisolid agar chemotaxis assays were performed on Brucella broth plates supplemented with 0.35% Bacto Agar, 2.5% FBS, 50 µg/mL cycloheximide, 10 µg/mL vancomycin, 5 µg/mL cefsulodin, 2.5 units/mL polymyxin B, 5 µg/mL trimethoprim, and 8 µg/mL amphotericin B. Plates were allowed to set for 2–3 days at room temperature before inoculation to remove excess moisture, inoculated from cultures grown on CHBA plates, incubated at 37°C under microaerobic conditions, and were imaged after 3, 5, and 7 days of incubation using the BioRad ChemiDoc XRS + imaging system. For isolation of Mig$^+$ suppressor mutant colonies, samples were picked from the outer edge of the expanded *H. pylori* mutant colonies after 4–5 days of growth. These samples were restreaked on CHBA plates and colony-purified.

Next-generation sequencing analysis

To purify genomic DNA for whole-genome sequencing, *H. pylori* G27 wild-type, *cheV1* mutant, and four Mig$^+$ suppressors were grown on CHBA plates supplemented with chloramphenicol. Genomic DNA was purified using the Promega Wizard Genomic DNA Purification Kit using the protocol for Gram-negative bacteria provided by the manufacturer and sent for MiSeq sequencing at the UC Davis fee-for-service facility.

Whole-genome sequencing (WGS) through MiSeq resulted in 2 × 300 paired-end reads. To proceed further with next-generation sequencing (NGS) analysis, these reads were first checked for quality using FastQC v0.11.5 (https://www.bioinformatics.babraham.ac.uk/projects/fastqc/) to determine their quality scores and then checked for the presence of Illumina sequencing adapters. BBDuk v37.25 (https://sourceforge.net/projects/bbmap/) was used to trim Illumina TruSeq DNA adapters from the right end using a K-mer length of 15–27. BBDuk was also used to trim low-quality bases from the 3′-end of the reads, removing bases lower than a quality score of Q20. Finally, reads less than 100 bp were discarded. A quality score of Q20 was chosen as it corresponds to a 99% inferred base call accuracy by the sequencer. https://www.illumina.com/science/technology/next-generation-sequencing/plan-experiments/quality-scores.html

To determine variations through WGS data generated from the four Mig$^+$ variants, Geneious R11 (Biomatters Ltd) (https://www.geneious.com) was used to map the quality-controlled reads from each to the wild-type *H. pylori* G27 reference genome (21). Five iterations of mapping were used, with the medium-sensitivity and high-sensitivity settings to confirm the results obtained were consistent and accurate. After mapping, variants were called using Geneious R11's Find Variations/SNP function, with a variant frequency of at least 75%, maximum variant *P*-value of 10^–6, and minimum strand-bias *P*-value set to 10^–5 when exceeding 65% bias.

PCR primer design and DNA sequencing

PCR primers were designed using Geneious R11 (Biomatters Ltd). To confirm the location of SNPs observed in whole-genome sequencing, the region containing the gene HPG27_252 was amplified using primers 277,426F (5′-CCTTTAAGCGACGGGTGGTT) and 278,017R (5′-TTGCACCAACAGCCCTTCAT) in wild-type *H. pylori* G27, *H. pylori* G27 Δ*cheV1* mutant, or Mig$^+$ Δ*cheV1::cat* colonies 5, 6, 8, and 11. Of note, there are two annotations of

the G27 genome: the original one, published in Baltrus *et al*. and denoted as "submitter" at the NCBI (https://www.ncbi.nlm.nih.gov/datasets/genome/?taxon=563041), and an auto-reannotation of the original G27 genome to create gene HPG27_RS01370, which is classified as a pseudogene. To confirm the knockout of HPG27_252 after transformation in the *H. pylori* G27 *cheV1* mutant, the surrounding region was amplified using primers HP_synDNA_277082F (5′-TGTGGTTTATGCACAACGCC) and HP_synDNA_279488R (5′-TG TAATGCCCGGACAGCTTT). Genomic DNA from these transformed cells was obtained following the protocol in the Promega Wizard Genomic DNA Purification Kit (Cat# A1120).

Construction of ΔHPG27_252::aphA3 mutants and complementation plasmids

H. pylori HPG27_252 mutants were constructed by natural transformation with plasmid pHPG27_252::*aphA3* DNA into *H. pylori* Δ*cheV1::cat* (Table S2), followed by selection for kanamycin resistance. pHPG27_252::*aphA3* was constructed synthetically (Genewiz) to knockout HPG27_252 by replacement with *aph*A3m, leaving a 24 bp and 19 bp of the original gene remaining at the 5′-end and 3′-end, respectively. Successful mutants were confirmed by PCR using primers flanking HPG27_252 (277320F (GCAAAGCGTGGTGGTT AGTG) and 277980R (GCAAAGCGTGGTGGTTAGTG) and sent for Sanger sequencing and stored as strain KO1700 (Table S2).

To create the complementing plasmid pILL2157-GFP-PilO, the full sequence of *hpG27_252* (540 bp) was amplified by PCR with primers XL140/141; all primer sequences in (22) using G27 genomic DNA as a template. The sequence of *gfp* without its stop codon was cloned from plasmid pEGFP-N2 using PCR with the primer pair XL138/XL139. To create a 5-glycine linker between GFP and HPG27_252, the sequences TCCGCCTCCGC CTCC and GGAGGCGGAGGCGGA were included in the primers XL139 (reverse complement of *gfp*) and XL140 (forward primer of hpG27_252), respectively. The amplified *gfp* and *hpG27_252* were further used as templates to perform PCR with the primer pair XL140/XL138. The resulting *gfp-hpG27_252* construct was purified, cleaned using the GFX PCR DNA and Gel Band Purification Kit (Thermo Fisher), digested by restriction enzymes NdeI and BamHI (New England Biolabs), and ligated into plasmid pILL2157 (38) digested by the same restriction enzymes. The resulting plasmid pILL2157-GFP-PilO (22) was transformed into *E. coli* DH10B (Table S2) and verified by sequencing. The N-terminal fusion of *gfp* with hpG27_252 was created by amplifying the sequence of *hpG27_252* without its stop codon from *H. pylori* G27 genomic DNA with primers XL142/XL143; full-length *gfp* was amplified with primers XL144/XL145 from plasmid pEGFN-N2. The two products were fused together with a 5-glycine linker, as mentioned previously, by PCR with primers XL142/XL245. The resulting PCR fragment was cleaned and introduced into plasmid pILL2157 used in similar processes as described above to create pILL2157-PilO-GFP (KO1786).

Plasmids were treated with the G27 cell-free extract to methylate, as described (39), and then 40 µg of treated plasmids were used to transform *H. pylori* G27 strains using chloramphenicol selection. Positive colonies were verified by repurifying plasmids and observing under a fluorescence microscope using GFP filters. These transformations resulted in the following strains:

Bioinformatics analysis of HPG27_252

Gene and protein sequences were obtained from the UCSC Microbial genome browsers. The operon structure was obtained from Sharma *et al*. (30), as visualized in the UCSC 26695 genome browser (40). Transmembrane domain and topology predictions were done with DeepTMHMM (41). Remote homology detection was done using HHpred at the MPI Bioinformatics Toolkit (27). The corrected protein sequence of *H. pylori* G27 PilO (HPG27_252) was used for sequence alignment with *P. aeruginosa* PilO, obtained from searching the UniProt database for PilO, resulting in *P. aeruginosa* PilO (G3XD51). The Needle program (https://www.ebi.ac.uk/Tools/psa/emboss_needle/) was

used to perform the pairwise protein sequence alignment with default parameters. The secondary structure of *P. aeruginosa* PilO was predicted by AlphaFold2 (42, 43).

Microscopic analysis of live cell tracking and fluorescence

For live cell tracking assays, liquid cultures of *H. pylori* were grown overnight in BB10, diluted to OD_{600}s between 0.2 and 0.3 the next day in fresh BB10, and filmed immediately under a microscope. Movies were captured using a Nikon Eclipse E600 microscope connected to a Hamamatsu 1394 ORCA-285S camera using a 20× phase-contrast objective and μManager (44). One minute of the video was captured with an approximate frame rate of 13 frames per second. These movies were then analyzed in 3-s intervals using ImageJ v1.53 (45) for flagellar reversals/direction changes, which were characterized as a sharp change in cell direction. A total of 50 cells were quantified for each strain used for this assay.

Subcellular localization of the PilO fused to GFP was from cells grown in liquid BB10 cultures with 1 mM IPTG. Cells were observed using a Nikon ECLIPSE E600 microscope, using GFP fluorescent filters under 100X oil immersion. Fluorescence and phase images were obtained using a Hamamatsu C7472-95 digital camera controlled by μManager software (Version 1.4.22).

Growth analysis

Liquid overnight cultures of wild-type *H. pylori* G27, *cheV1* mutant, and Mig^+ colony 5 were grown in BB10. After overnight growth, the cultures were diluted to an OD_{600} of 0.250 using fresh BB10, and OD600 values were measured every 3 h for 12 h.

ACKNOWLEDGMENTS

The authors would like to thank members of the Ottemann Lab, with special thanks to Skander Hathroubi and Kevin Johnson for their continued support throughout this project. We would also like to thank Andrew Kebbel for his guidance through the NGS data analysis process and Thomas Hake for helping with certain computational statistical analyses in this study.

The described project was supported by the National Institutes of Health National Institute of Allergy and Infectious Disease (NIAID) grant numbers R01 AI116946 and R01 AI164682 (to K.M.O.) and a student fellowship from the China Scholarship Council to X.L., with the project number 201904910692.

The funders had no role in study design, data collection, and interpretation or the decision to submit the work for publication.

AUTHOR AFFILIATION

[1]Department of Microbiology and Environmental Toxicology, UC Santa Cruz, Santa Cruz, California, USA

AUTHOR ORCIDs

Jashwin Sagoo http://orcid.org/0009-0000-0792-153X
Xiaolin Liu http://orcid.org/0000-0001-5891-4559
Karen M. Ottemann http://orcid.org/0000-0001-6265-7401

FUNDING

Funder	Grant(s)	Author(s)
HHS | NIH | National Institute of Allergy and Infectious Diseases (NIAID)	AI116946	Jashwin Sagoo Samar Abedrabbo Karen M. Ottemann

Funder	Grant(s)	Author(s)
HHS | NIH | National Institute of Allergy and Infectious Diseases (NIAID)	AI164682	Xiaolin Liu Karen M. Ottemann
China Scholarship Council (CSC)	201904910692	Xiaolin Liu

AUTHOR CONTRIBUTIONS

Jashwin Sagoo, Conceptualization, Formal analysis, Investigation, Methodology, Writing – original draft, Writing – review and editing | Samar Abedrabbo, Conceptualization, Formal analysis, Investigation, Writing – original draft, Writing – review and editing | Xiaolin Liu, Investigation, Methodology, Writing – original draft.

ADDITIONAL FILES

The following material is available online.

Supplemental Material

Supplemental material (JB00406-23-S0001.docx). Figures S1 to S3; Tables S1 and S2.
Video S1 (JB00406-23-S0002.avi). Movie S1.
Video S2 (JB00406-23-S0003.avi). Movie S2.
Video S3 (JB00406-23-S0004.avi). Movie S3.

REFERENCES

1. Colin R, Ni B, Laganenka L, Sourjik V. 2021. Multiple functions of flagellar motility and chemotaxis in bacterial physiology. FEMS Microbiol Rev 45:fuab038. https://doi.org/10.1093/femsre/fuab038
2. Matilla MA, Gavira JA, Krell T. 2023. Accessing nutrients as the primary benefit arising from chemotaxis. Curr Opin Microbiol 75:102358. https://doi.org/10.1016/j.mib.2023.102358
3. Keegstra JM, Carrara F, Stocker R. 2022. The ecological roles of bacterial chemotaxis. Nat Rev Microbiol 20:491–504. https://doi.org/10.1038/s41579-022-00709-w
4. Ortega Á, Zhulin IB, Krell T. 2017. Sensory repertoire of bacterial chemoreceptors. Microbiol Mol Biol Rev 81:e00033-17. https://doi.org/10.1128/MMBR.00033-17
5. Wuichet K, Zhulin IB. 2010. Origins and diversification of a complex signal transduction system in prokaryotes. Sci Signal 3:ra50. https://doi.org/10.1126/scisignal.2000724
6. Alexander RP, Lowenthal AC, Harshey RM, Ottemann KM. 2010. CheV: cheW-like coupling proteins at the core of the chemotaxis signaling network. Trends Microbiol 18:494–503. https://doi.org/10.1016/j.tim.2010.07.004
7. Piñas GE, Frank V, Vaknin A, Parkinson JS. 2016. The source of high signal cooperativity in bacterial chemosensory arrays. Proc Natl Acad Sci USA 113:3335–3340. https://doi.org/10.1073/pnas.1600216113
8. Huang Z, Pan X, Xu N, Guo M. 2019. Bacterial chemotaxis coupling protein: structure, function and diversity. Microbiol Res 219:40–48. https://doi.org/10.1016/j.micres.2018.11.001
9. Abedrabbo S, Castellon J, Collins KD, Johnson KS, Ottemann KM. 2017. Cooperation of two distinct coupling proteins creates chemosensory network connections. Proc Natl Acad Sci USA 114:2970–2975. https://doi.org/10.1073/pnas.1618227114
10. Malfertheiner P, Camargo MC, El-Omar E, Liou J-M, Peek R, Schulz C, Smith SI, Suerbaum S. 2023. *Helicobacter pylori* infection. Nat Rev Dis Primers 9:19. https://doi.org/10.1038/s41572-023-00431-8
11. Crowe SE. 2019. *Helicobacter pylori* infection. N Engl J Med 381:588–589. https://doi.org/10.1056/NEJMc1905439
12. Johnson KS, Ottemann KM. 2018. Colonization, localization, and inflammation: the roles of *H. pylori* chemotaxis *in vivo*. Curr Opin Microbiol 41:51–57. https://doi.org/10.1016/j.mib.2017.11.019
13. Keilberg D, Ottemann KM. 2016. How *Helicobacter pylori* senses, targets and interacts with the gastric epithelium. Environ Microbiol 18:791–806. https://doi.org/10.1111/1462-2920.13222
14. Terry K, Williams SM, Connolly LL, Ottemann KM. 2005. Chemotaxis plays multiple roles during *Helicobacter pylori* animal infection. Infect Immun 73:803–811. https://doi.org/10.1128/IAI.73.2.803-811.2005
15. Lowenthal AC, Simon C, Fair AS, Mehmood K, Terry K, Anastasia S, Ottemann KM. 2009. A fixed-time diffusion analysis method determines that the three *cheV* genes of *Helicobacter pylori* differentially affect motility. Microbiology (Reading) 155:1181–1191. https://doi.org/10.1099/mic.0.021857-0
16. Pittman MS, Goodwin M, Kelly DJ. 2001. Chemotaxis in the human gastric pathogen *Helicobacter pylori*: different roles for cheW and the three CheV paralogues, and evidence for CheV2 phosphorylation. Microbiology (Reading) 147:2493–2504. https://doi.org/10.1099/00221287-147-9-2493
17. Jiménez-Pearson M-A, Delany I, Scarlato V, Beier D. 2005. Phosphate flow in the chemotactic response system of *Helicobacter pylori*. Microbiology (Reading) 151:3299–3311. https://doi.org/10.1099/mic.0.28217-0
18. Wolfe AJ, Berg HC. 1989. Migration of bacteria in semisolid agar. Proc Natl Acad Sci USA 86:6973–6977. https://doi.org/10.1073/pnas.86.18.6973
19. Andermann TM, Chen Y-T, Ottemann KM. 2002. Two predicted chemoreceptors of *Helicobacter pylori* promote stomach infection. Infect Immun 70:5877–5881. https://doi.org/10.1128/IAI.70.10.5877-5881.2002
20. Terry K, Go AC, Ottemann KM. 2006. Proteomic mapping of a suppressor of non-chemotactic cheW mutants reveals that *Helicobacter pylori* contains a new chemotaxis protein. Mol Microbiol 61:871–882. https://doi.org/10.1111/j.1365-2958.2006.05283.x
21. Baltrus DA, Amieva MR, Covacci A, Lowe TM, Merrell DS, Ottemann KM, Stein M, Salama NR, Guillemin K. 2009. The complete genome sequence of *Helicobacter pylori* strain G27. J Bacteriol 191:447–448. https://doi.org/10.1128/JB.01416-08
22. Liu X, Tachiyama S, Zhou X, Mathias RA, Bonny SQ, Khan MF, Xin Y, Roujeinikova A, Liu J, Ottemann KM. 2024. Bacterial flagella hijack type IV pili proteins to control motility. Proc Natl Acad Sci USA 121:e2317452121. https://doi.org/10.1073/pnas.2317452121
23. Lertsethtakarn P, Howitt MR, Castellon J, Amieva MR, Ottemann KM. 2015. *Helicobacter pylori* CheZ and ChePep form a novel chemotaxis - regulatory complex distinct from the core chemotaxis signaling proteins and the flagellar motor. Mol Microbiol 97:1063–1078. https://doi.org/10.1111/mmi.13086

24. Tomb JF, White O, Kerlavage AR, Clayton RA, Sutton GG, Fleischmann RD, Ketchum KA, Klenk HP, Gill S, Dougherty BA, et al. 1997. The complete genome sequence of the gastric pathogen *Helicobacter pylori*. Nature 388:539–547. https://doi.org/10.1038/41483
25. Sampaleanu LM, Bonanno JB, Ayers M, Koo J, Tammam S, Burley SK, Almo SC, Burrows LL, Howell PL. 2009. Periplasmic domains of *Pseudomonas aeruginosa* PilN and PilO form a stable heterodimeric complex. J Mol Biol 394:143–159. https://doi.org/10.1016/j.jmb.2009.09.037
26. Leighton TL, Yong DH, Howell PL, Burrows LL. 2016. Type IV pilus alignment subcomplex proteins PilN and PilO form homo- and heterodimers *in vivo*. J Biol Chem 291:19923–19938. https://doi.org/10.1074/jbc.M116.738377
27. Zimmermann L, Stephens A, Nam S-Z, Rau D, Kübler J, Lozajic M, Gabler F, Söding J, Lupas AN, Alva V. 2018. A completely reimplemented MPI bioinformatics toolkit with a new HHpred server at its core. J Mol Biol 430:2237–2243. https://doi.org/10.1016/j.jmb.2017.12.007
28. Alm RA, Ling LS, Moir DT, King BL, Brown ED, Doig PC, Smith DR, Noonan B, Guild BC, deJonge BL, Carmel G, Tummino PJ, Caruso A, Uria-Nickelsen M, Mills DM, Ives C, Gibson R, Merberg D, Mills SD, Jiang Q, Taylor DE, Vovis GF, Trust TJ. 1999. Genomic-sequence comparison of two unrelated isolates of the human gastric pathogen *Helicobacter pylori*. Nature 397:176–180. https://doi.org/10.1038/16495
29. Draper JL, Hansen LM, Bernick DL, Abedrabbo S, Underwood JG, Kong N, Huang BC, Weis AM, Weimer BC, van Vliet AHM, Pourmand N, Solnick JV, Karplus K, Ottemann KM. 2017. Fallacy of the unique genome: sequence diversity within single *Helicobacter pylori* strains. mBio 8:e02321-16. https://doi.org/10.1128/mBio.02321-16
30. Sharma CM, Hoffmann S, Darfeuille F, Reignier J, Findeiss S, Sittka A, Chabas S, Reiche K, Hackermüller J, Reinhardt R, Stadler PF, Vogel J. 2010. The primary transcriptome of the major human pathogen *Helicobacter pylori*. Nature 464:250–255. https://doi.org/10.1038/nature08756
31. McCallum M, Burrows LL, Howell PL. 2019. The dynamic structures of the type IV pilus. Microbiol Spectr 7:7. https://doi.org/10.1128/microbiolspec.PSIB-0006-2018
32. Naskar S, Hohl M, Tassinari M, Low HH. 2021. The structure and mechanism of the bacterial type II secretion system. Mol Microbiol 115:412–424. https://doi.org/10.1111/mmi.14664
33. Partridge JD, Harshey RM. 2020. Investigating flagella-driven motility in *Escherichia Coli* by applying three established techniques in a series. J Vis Exp. https://doi.org/10.3791/61364
34. Lertsethtakarn P, Ottemann KM. 2010. A remote CheZ orthologue retains phosphatase function. Mol Microbiol 77:225–235. https://doi.org/10.1111/j.1365-2958.2010.07200.x
35. Mohari B, Licata NA, Kysela DT, Merritt PM, Mukhopadhay S, Brun YV, Setayeshgar S, Fuqua C. 2015. Novel pseudotaxis mechanisms improve migration of straight-swimming bacterial mutants through a porous environment. mBio 6:e00005. https://doi.org/10.1128/mBio.00005-15
36. Nieto V, Partridge JD, Severin GB, Lai R-Z, Waters CM, Parkinson JS, Harshey RM. 2019. Under elevated c-di-GMP in *Escherichia coli*, YcgR alters flagellar motor bias and speed sequentially, with additional negative control of the flagellar regulon via the adaptor protein RssB. J Bacteriol 202:e00578-19. https://doi.org/10.1128/JB.00578-19
37. Censini S, Lange C, Xiang Z, Crabtree JE, Ghiara P, Borodovsky M, Rappuoli R, Covacci A. 1996. *cag*, a pathogenicity island of *Helicobacter pylori*, encodes type I-specific and disease-associated virulence factors. Proc Natl Acad Sci USA 93:14648–14653. https://doi.org/10.1073/pnas.93.25.14648
38. Boneca IG, Ecobichon C, Chaput C, Mathieu A, Guadagnini S, Prévost M-C, Colland F, Labigne A, de Reuse H. 2008. Development of inducible systems to engineer conditional mutants of essential genes of *Helicobacter pylori*. Appl Environ Microbiol 74:2095–2102. https://doi.org/10.1128/AEM.01348-07
39. Donahue JP, Israel DA, Peek RM, Blaser MJ, Miller GG. 2000. Overcoming the restriction barrier to plasmid transformation of *Helicobacter pylori*. Mol Microbiol 37:1066–1074. https://doi.org/10.1046/j.1365-2958.2000.02036.x
40. Chan PP, Holmes AD, Smith AM, Tran D, Lowe TM. 2012. The UCSC archaeal genome browser: 2012 update. Nucleic Acids Res 40:D646–52. https://doi.org/10.1093/nar/gkr990
41. Hallgren J, Tsirigos KD, Pedersen MD, Almagro Armenteros JJ, Marcatili P, Nielsen H, Krogh A, Winther O. 2022. DeepTMHMM predicts alpha and beta transmembrane proteins using deep neural networks. Bioinformatics. https://doi.org/10.1101/2022.04.08.487609
42. Jumper J, Evans R, Pritzel A, Green T, Figurnov M, Ronneberger O, Tunyasuvunakool K, Bates R, Žídek A, Potapenko A, et al. 2021. Highly accurate protein structure prediction with alphafold. Nature 596:583–589. https://doi.org/10.1038/s41586-021-03819-2
43. Varadi M, Anyango S, Deshpande M, Nair S, Natassia C, Yordanova G, Yuan D, Stroe O, Wood G, Laydon A, et al. 2022. Alphafold protein structure database: massively expanding the structural coverage of protein-sequence space with high-accuracy models. Nucleic Acids Res 50:D439–D444. https://doi.org/10.1093/nar/gkab1061
44. Edelstein AD, Tsuchida MA, Amodaj N, Pinkard H, Vale RD, Stuurman N. 2014. Advanced methods of microscope control using μManager software. J Biol Methods 1:e10. https://doi.org/10.14440/jbm.2014.36
45. Schneider CA, Rasband WS, Eliceiri KW. 2012. NIH image to imageJ: 25 years of image analysis. Nat Methods 9:671–675. https://doi.org/10.1038/nmeth.2089